ENTRY, DESCENT, AND LANDING PERFORMANCE FOR A MID-LIFT-TO-DRAG RATIO VEHICLE AT MARS

Breanna J. Johnson,[*] Ellen M. Braden,[†] Ronald R. Sostaric,[‡] Christopher J. Cerimele,[§] and Dr. Ping Lu[**]

In an effort to mature the design of the Mid-Lift-to-Drag ratio Rigid Vehicle (MRV) candidate of the NASA Evolvable Mars Campaign (EMC) architecture study, end-to-end six-degree-of-freedom (6DOF) simulations are needed to ensure a successful entry, descent, and landing (EDL) design. The EMC study is assessing different vehicle and mission architectures to determine which candidate would be best to deliver a 20 metric ton payload to the surface of Mars. Due to the large mass payload and the relatively low atmospheric density of Mars, all candidates of the EMC study propose to use Supersonic Retro-Propulsion (SRP) throughout the descent and landing phase, as opposed to parachutes, in order to decelerate to a subsonic touchdown. This paper presents a 6DOF entry-to-landing performance and controllability study with sensitivities to dispersions, particularly in the powered descent and landing phases.

INTRODUCTION

Studies for human missions to Mars have shown that there is a need to design vehicles capable of delivering heavier payloads to the surface of Mars than has previously been attempted. To date, all fully successful Mars landings have been completed for payloads of about 1 metric ton (mt) or less, but studies have shown that payloads of 15-40 mt of delivery mass to the surface are needed for human missions.[1] Robotic missions to Mars have relied on parachutes during the descent phase. However, the payload requirement for this study increases the difficulty of achieving a successful Mars landing. As the payload and vehicle mass increase, the vehicle's ballistic coefficient can be reduced in order to begin deceleration from entry to subsonic speeds higher in the atmosphere, allowing for more time to correct for possible underestimated atmospheric conditions.[2] For the lower ballistic coefficient robotic vehicles, final descent phases were achieved by decreasing the drag coefficient and ballistic coefficient with parachutes. However with current technology, parachutes able to carry the loads for a vehicle of this mass would need to be of an impractically large surface area to ensure successful deployment and deceleration, hence the need for the engine-powered supersonic-retro-propulsion (SRP) descent and landing phase.

To address the technology gap in human Mars entry, descent, and landing (EDL) for large bodied vehicles, NASA has formulated the Evolvable Mars Campaign (EMC) to define the risks and

[*] Aerospace Engineer, Flight Mechanics and Trajectory Design, NASA Johnson Space Center, Houston, TX, 77058.
[†] Aerospace Engineer, Flight Mechanics and Trajectory Design, NASA Johnson Space Center, Houston, TX, 77058.
[‡] Aerospace Engineer, Flight Mechanics and Trajectory Design, NASA Johnson Space Center, Houston, TX, 77058.
[§] EDL Domain Lead, Flight Mechanics and Trajectory Design, NASA Johnson Space Center, Houston, TX, 77058.
[**] Chair, Department of Aerospace Engineering, San Diego State University, San Diego, CA, 92182.

benefits of candidate future vehicles that would be capable of safely delivering a 20 mt payload to the surface of Mars.[3] The payload requirement of 20 mt stems from the mass estimate of a Mars Ascent Vehicle (MAV) that would need to be transported for a future return mission. With a hypersonic lift-to-drag-ratio (L/D) of 0.54, the MRV is an intermediate approach between the winged Shuttle (L/D of 1.5), and a blunt-body capsule (typically L/D of 0.3 or less).[4] The MRV concept takes advantage of both the SLS payload fairing shape for increased payload volume and NASA's heritage with design, controls, construction, testing, and operations for rigid entry vehicles.

The nominal MRV trajectory includes a bank-angle-modulated guidance for the hypersonic entry and a simple gravity turn for the descent and landing phases as an initial assessment of the EDL control system approach. The gravity turn assumes that the thrust vector is aligned in the anti-velocity direction. It provides a quick and easy approach to performing an initial assessment of the descent and landing trajectory, along with a rough estimate of its associated propellant requirement. Future studies will include the Universal Powered Guidance (UPG) algorithm for comparison.[5] UPG is capable of quickly generating a fuel-optimal solution for a wide range of dispersed trajectories. It also has the advantage over gravity turn solutions of being able to fly to a chosen landing site target.

This paper examines the flight performance and robustness of the Mid-L/D Rigid Vehicle (MRV) by analyzing control system precision, controllability, and propellant usage for nominal and off-nominal trajectories using a gravity turn powered flight assumption.

NOMINAL END-TO-END TRAJECTORY

Nominal EDL trajectories were generated in three-degrees-of-freedom (3DOF) and six-degrees-of-freedom (6DOF) with the Johnson Space Center (JSC) Flight Analysis and Simulation Tool (FAST). In order to ensure that the MRV had a feasible control system capable of satisfactory performance throughout EDL, an FNPEG guided entry trajectory complete with a simple gravity turn powered descent and landing phase was created to showcase the vehicle's controllability. The gravity turn powered descent is guided by orienting the thrust vector in the opposite direction of the velocity vector as shown in Figure 1.

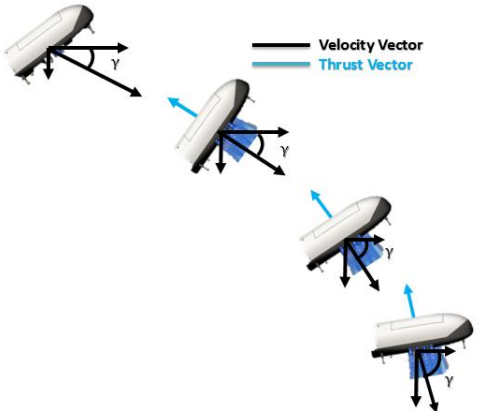

Figure 1. General Gravity Turn Diagram.

By thrusting in the direction opposite of the velocity vector, horizontal velocity is minimized until the only remaining velocity is vertical, due to the Mars gravitational acceleration. As the vehicle nears vertical descent, the flight path angle γ approaches -90 deg. For this study, two versions of gravity turn, constant acceleration and constant thrust, were examined in 3DOF. Once a preferred gravity turn strategy was determined, a fully end-to-end 6DOF trajectory was generated to test

vehicle controllability throughout EDL. All trajectories feature 8 main engines providing a combined maximum thrust level of 800 kN and nominal throttle of 80 %. Descent and landing was modeled with no aerodynamics since the main engines are assumed to likely dominate the aerodynamics. Modeling of SRP flow is nascent and has not yet been simulated for the MRV, so removing aerodynamics provides a conservative nominal trajectory (with respect to slowing the vehicle) until that interaction is modeled.

3DOF Entry Descent and Landing

The entry phase of flight begins after orbital insertion at an approximate altitude of 130 km and velocity of 4,700 m/s. Similar to previous Mars missions, the MRV would use coupled bank-angle steering during entry to reduce hypersonic speeds for a safe landing. FNPEG utilizes this bank angle steering during entry to guide the MRV to its target by rotating the lift vector around the velocity vector to minimize downrange and crossrange errors within mission constraints. Constraints that FNPEG can incorporate include limits on maximum g-loads, heating rate, dynamic pressure, and range targeting errors.[6] FNPEG targets a Powered Descent Initiation (PDI) condition to begin the SRP phase based on a desired energy, which is a combination of altitude and velocity. For the PDI condition, there exists a combination of altitude, velocity, flight path angle, and thrust that produces a soft landing gravity turn. This condition is critical for mission success and is different for each constant acceleration or constant thrust gravity turn case.

For a constant thrust descent, the vehicle targets a vertical phase initiation, at which point a second and final constant thrust is selected to complete the gravity turn to zero velocity and zero height. Using the 3DOF entry trajectory profile, a scan was generated to determine the necessary PDI energy condition of altitude and velocity to arrive at the vertical phase initiation conditions of 2.5 m/s at 12.5 m for the nominal total main engine thrust of 640 kN (80% of 800 kN). The vertical phase initiation energy was selected based on a representative fuel optimized trajectory solution.[4] The conditions at the start of powered descent are shown in Figures 2a and 2b. A varying altitude trigger is used to establish the conditions at the end of entry that would match the fuel optimized trajectory solution. The value of the altitude is shown on the x-axis. Figures 2c and 2d show the resulting powered flight trajectory possibilities for the varying altitude trigger. In Fig. 2c, the solutions to the left (lower altitude) represent valid, but non-fuel-optimal, resulting trajectories for the powered flight. PDI altitudes greater than the fuel optimal 7.28 km resulted in cases that reached 0 deg pitch before enough energy had been decreased. Because of this they would hover at too high of an altitude, where all propellant was used before desired conditions were reached. Figure 2d shows the associated propellant usage. The trend is increasing propellant usage with increasing altitude, however altitude triggers above the 7.28 km mark resulted in trajectories where all propellant was used due to the vehicle hovering. Again, altitudes greater than 7.28 are not valid solutions.

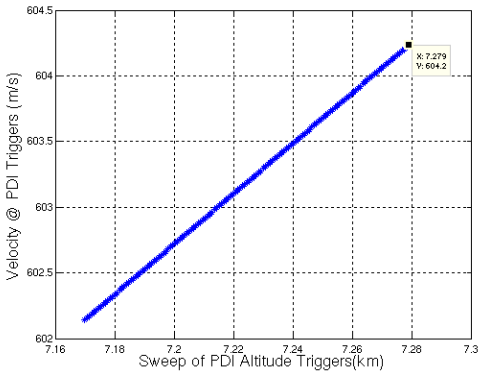

(a) Velocity at PDI vs. Altitude at PDI

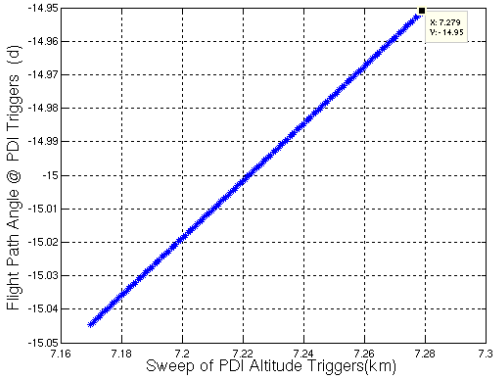

(b) Flight Path Angle at PDI vs. Altitude at PDI

* A section on mathematical notation is provided in the sequel

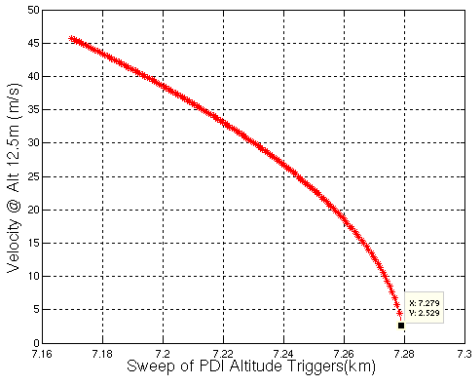

(c) Velocity at Vertical Descent vs. Altitude at PDI

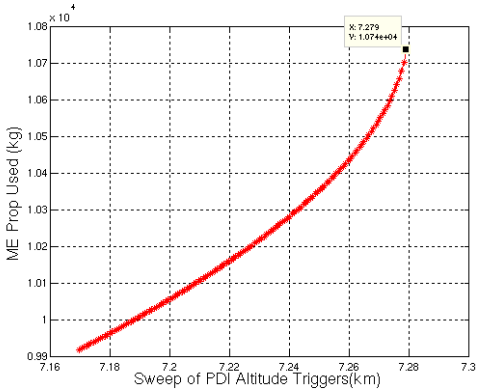

(d) ME Propellant Used at Vertical Descent vs. Altitude at PDI

Figure 2. PDI Initial Condition Scan

Following the gravity turn, a final phase was modeled. At the altitude of 12.5 m and velocity of 2.5 m/s, a new constant thrust level was chosen for the purely vertical descent to softly land at an approximate zero velocity. A similar scan was run to efficiently find that for a constant thrust gravity turn with a PDI energy of 7.28 km altitude, 604 m/s velocity, and -14.95 deg flight path angle, a final constant thrust of 184 kN (23% of 800 kN) was needed for a soft landing.

For a constant acceleration descent, the vehicle targets a zero velocity at zero altitude by analytically solving Equation 1 for the constant thrust acceleration or PDI altitude to begin the gravity turn.[7]

$$\left(\frac{a_T}{g}\right)^2 + sin\,\gamma_0 \left(\frac{V_0^2}{2h_0 g}\right)\frac{a_T}{g} - \left[\frac{V_0^2(1+\sin^2\gamma_0)}{4h_0 g} + 1\right] = 0 \qquad (1)$$

When solved, this equation yields only one positive root for negative flight path angles (γ_0), assuming that the thrusting acceleration is larger than the 3.711 m/s/s gravitational acceleration of Mars.* To allow for easier comparison to the constant thrust gravity turn, the acceleration of 10.9 m/s/s was chosen to ensure the same initial thrusts for both cases. A comparison of the end-to-end trajectories with constant thrust and constant acceleration gravity turn trajectory profiles is shown in Figure 3. Figures 3a and 3b shows overall agreement in Euler angle profiles, where the dotted lines represent the constant acceleration case and the solid lines represent the constant thrust case. The thrust profile show in Figure 3c highlights the 2 constant thrust commands for the constant thrust case and the continuously changing thrust command for the constant acceleration case. Figure 3d shows the end of both trajectories, where the constant acceleration case must begin before the constant thrust case to deplete the same amount of energy.

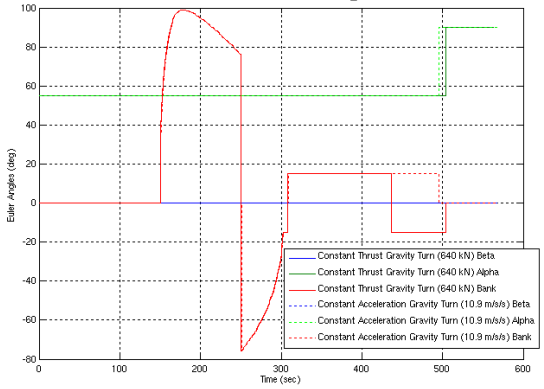

(a)Attitude Comparison (Sideslip, Angle of Attack, Bank)

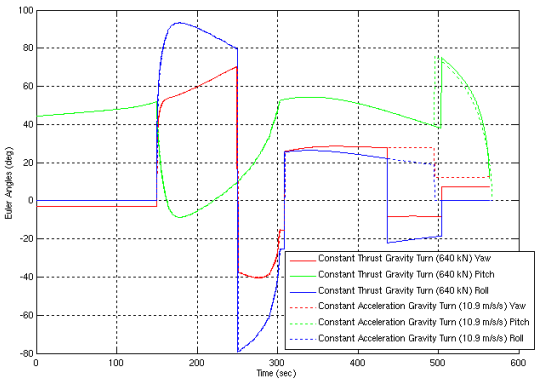

(b) Attitude Comparison (North-East-Down to Body)

* A section on mathematical notation is provided in the sequel

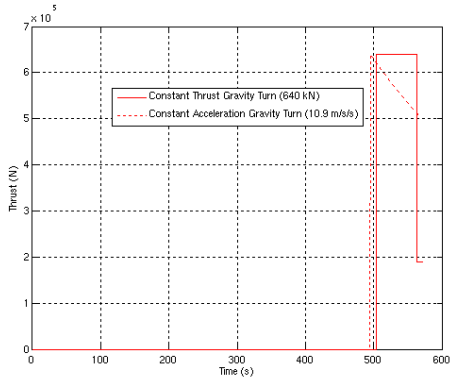

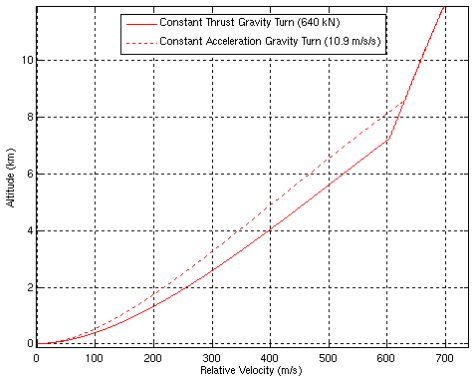

(c) Thrust Profile Comparison *(d) Altitude vs. Planet Relative Velocity Comparison*

Figure 3. Constant Thrust vs. Constant Acceleration Gravity Turn.

Constant thrust gravity turns are beneficial to main engines since limitations in throttle and throttle rates can be an issue in achieving a soft landing. However while constant acceleration gravity turns require variable throttle rates, they have better acceleration flight path angle rate control, allowing for a smoother continuous engine throttle profile. Additionally, they are generally more robust with uncertainties, since Equation 1 may be analytically solved throughout the trajectory. Higher acceleration gravity turns are the most fuel optimal. And the constant thrust case increases acceleration until the vertical descent (as shown in Figure 3d), but it also leaves less margin to correct for any atmospheric uncertainties, since they generally are larger later in the trajectory. For these reasons, a constant thrust descent was chosen to showcase the 6DOF end-to-end trajectory.

6DOF Entry Phase

During the entry phase, the MRV uses a Reaction Control System (RCS) of jets along with aerosurfaces to command to the FNPEG provided bank angle commands. The MRV RCS shown in Figure 4 utilizes twenty 4,448 N jets for large torques and eight 2,224 N jets for finer attitude control throughout EDL.

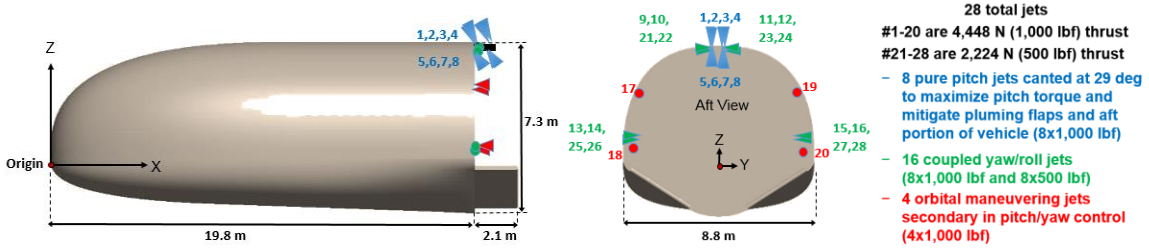

Figure 4. RCS Jet Locations.

The MRV takes advantage of its aerodynamic stability characteristics and split flap aerosurfaces, which can effectively act as a coupled elevon and rudder, to achieve satisfactory attitude control with minimal propellant usage. [8] The placement of the center of mass/center of gravity (CG) determines the trim angles at which the vehicle is statically stable, ensuring that any disturbance torque on the system would produce a complementary restoring moment back to trim. The equations of motion are defined in Equations 2-4, where gains are determined by a desirable frequency and damping ratio response. *

$$\tau_x = I_x\dot{p} = C_{l_\beta}\beta\bar{q}SL + m_x\left(-K_\beta\beta - K_p p + K_p r_c COT\alpha\right) + C_{l_{\delta_a}}\delta_a\bar{q}SL \quad (2)$$

$$\tau_y = I_y\dot{q} = C_{m_\alpha}\alpha\bar{q}SL + m_y\left(K_\alpha(\alpha_c - \alpha) - K_q q\right) + C_{m_{\delta_e}}\delta_e\bar{q}SL \quad (3)$$

$$\tau_z = I_z\dot{r} = C_{n_\beta}\beta\bar{q}SL + m_z(K_r r_c - K_r r) + C_{n_{\delta_a}}\delta_a\bar{q}SL \quad (4)$$

* A section on mathematical notation is provided in the sequel

The equations of motion include the moment from expected static stability aerodynamic contributions, the moment from the RCS control system, and the moment from the aerosurfaces. Aerosurface deflection moments are further defined by Equations 5-6.

$$\delta_e = K_{\alpha_{AS}}(\alpha_c - \alpha) - K_{q_{AS}} q \tag{5}$$

$$\delta_a = K_{p_{AS}}(r_c \cot \alpha - p) - K_{\beta_{AS}} \beta \tag{6}$$

Gains are determined for a desired damping and frequency response when solving the linearized second order differential equations

$$\ddot{\alpha} + 2\xi\omega_{SP}\dot{\alpha} + \omega_{SP}^2 \alpha = 0 \tag{7}$$

$$I_z \ddot{\beta} + k_{\dot{\beta}} \dot{\beta} + C'_{n\beta_{dyn}} \beta \bar{q} S L = constant \tag{8}$$

Bank angle commands provided by FNPEG are managed primarily by the RCS with flap assistance. Comparison of the 3DOF to 6DOF trajectories are provided in Figure 5 and show satisfactory trajectory agreement. The bank angle profiles for the 3DOF and 6DOF cases shown in Figure 5c differ due to the fact that guidance is running at the same high frequency as the controls (25 Hz) for the 3DOF trajectory, while the 6DOF trajectory uses a more realistic guidance frequency of 1 Hz. In addition, 3DOF uses instantaneous tracking, where the bank angles perfectly follow the guidance commands. Since FNPEG is a closed-loop guidance, the 3DOF and 6DOF guidance commands will not necessarily align perfectly. These differences, in addition to thrust limitations of the 6DOF control system, impact the G-load and flight path angle profiles as well.

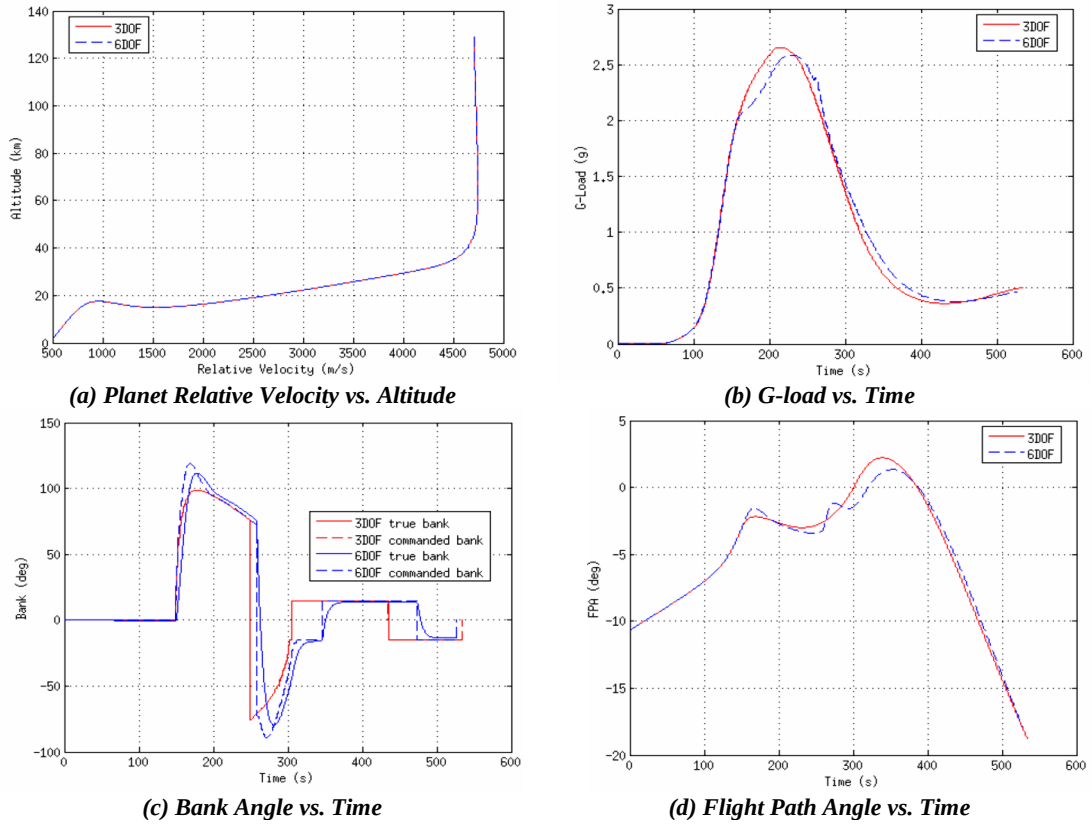

(a) Planet Relative Velocity vs. Altitude

(b) G-load vs. Time

(c) Bank Angle vs. Time

(d) Flight Path Angle vs. Time

Figure 5. 3DOF vs. 6DOF Entry Trajectory

6DOF Descent and Landing Phase

The descent and landing control system utilizes both the main engines and RCS jets and is designed to control large angle changes. For the nominal trajectory's gravity turn, a 35 deg change in pitch is necessary to orient the vehicle attitude away from the entry trim angle of attack and orient the main engines in the direction perpendicular to the velocity vector. While the RCS jets are capable of this large pitch angle change for the nominal trajectory, they were unable to achieve this in the presence of a CG offset at the corners of the expected CG box as shown in Figure 6.

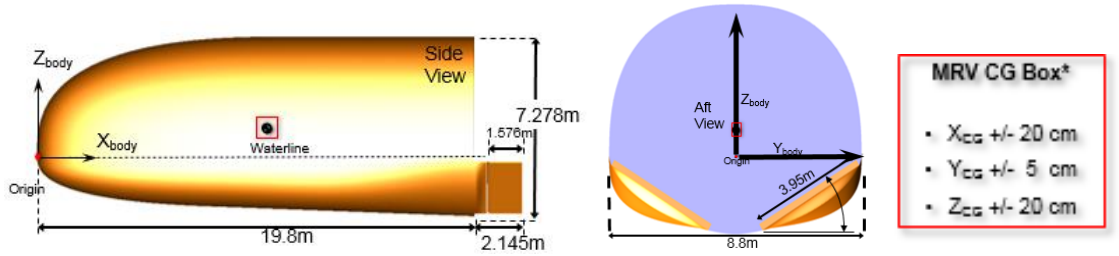

Figure 6. CG Box Definition.

Thus, the main engines are required to not only thrust against the velocity vector, but also provide a constant stabilizing torque to counteract any off-nominal conditions. They are used to compensate for large dispersions, such as CG offsets, initiate large attitude changes, and control attitude accelerations. Attitude control is divided between the main engines and the RCS. While the RCS use a Proportional-Derivative (PD) controller similar to the entry controller detailed in Equations 2-6, the main engines use a modified PD controller that also controls for the angular accelerations.

A diagram of the main engines is shown in Figure 7. All engines are canted 10 deg from vertical. The port and starboard main engines numbered 1 and 4 are used for pitch control. The two inner main engines, port and starboard main engines 2 and 3, are used for roll control. The main engines are not used for yaw control since this is adequately supported by the RCS jets. These engines can control vehicle attitude only to the precision to which they can be throttled. It is important to ensure that the main engines and RCS do not fight each other, so inhibit flags are used in the main engine logic. The RCS is used to dampen attitude rates and hold attitude once the main engines are inhibited.

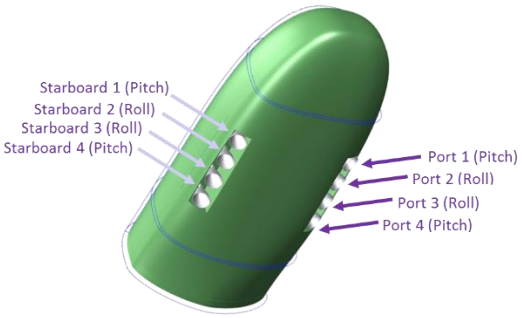

Figure 7. Main Engine Locations.

The control strategy for descent and landing was originally prototyped in the dynamics simulation software Automated Dynamic Analysis of Mechanical Systems (ADAMS) to better study the dynamics of the system before implemented in FAST. The controls logic consists of three segments. Segment 1 is main engine start-up and attitude hold. RCS jets are necessary to eliminate

any residual errors from entry and to eliminate disturbance torques due to main engine placement about the CG or dispersions in start-up transients. To compensate for the initial thrust dispersions and CG offsets in Segment 1, a PID controller using the angle errors, angular rates, and angular accelerations is used to calculate the main engine commanded torques for roll and pitch control, as shown in Equations 9 and 10, where θ represents the pitch angle and μ represents the roll angle between the North-East-Down (NED) and body frames of reference.

$$\tau_{MEx} = (K_{\mu}(\mu_c - \mu) - K_p\, p + K_{\dot{p}}\, \dot{p}\,)/2.0 \quad (9)$$

$$\tau_{MEy} = (K_{\theta}(\theta_c - \theta) - K_q\, q + K_{\dot{q}}\, \dot{q}\,)/2.0 \quad (10)$$

The pitch commanded torque is divided by two because the pitch main engines are used in pairs, the forward engines and the rear engines, and the roll commanded torque is divided by two because the roll main engines are also used in pairs, port and starboard main engines 2 and 3. The gains are chosen so that dampening the rates and accelerations is the control system priority. They are not reliant on aerodynamic stability derivatives like during entry, since the descent and landing phase is currently modeled with no aerodynamics.

Segment 2 begins the commanded pitch up to a 90 deg angle of attack from the nominal trim angle-of-attack of 55 deg while keeping the yaw and roll attitudes constant. Bank angle and Sideslip are commanded to zero. The same Equation 10 from Segment 1 is used in Segment 2 for pitch control. The pitch main engines are throttled to create a pitch rate in the positive pitching direction. For a positive angle change the thrust of the forward engines is increased and the thrust on the rear engines is decreased. Once the pitch rate reaches a user defined pitch rate (2 deg/s for the nominal trajectory), the pitch main engines are throttled to create a pitch rate in the negative pitching direction, dampening out the pitch acceleration, until the predicted pitch acceleration becomes zero. The final level of thrust will be returned to thrust values similar to the original thrust levels if no dispersions are present before inhibition. When the pitch is within a user defined threshold of the commanded pitch angle, the RCS is used to dampen out the pitch rate and maintain the 90 deg pitch angle. Throughout this segment the RCS jets are maintaining the yaw and roll attitude. In Segment 3, all main engines are inhibited and RCS is used to maintain attitude.

Including throttle rates was an important detail to increase control system fidelity since the main engines are realistically incapable of instantaneously producing the nominal thrust level. Figure 8a-8b show main engine thrust profiles for a higher fidelity throttle rate limited control profile. The main engine startup throttle rate is 56 %/s and the nominal throttle rate is 80%/s.

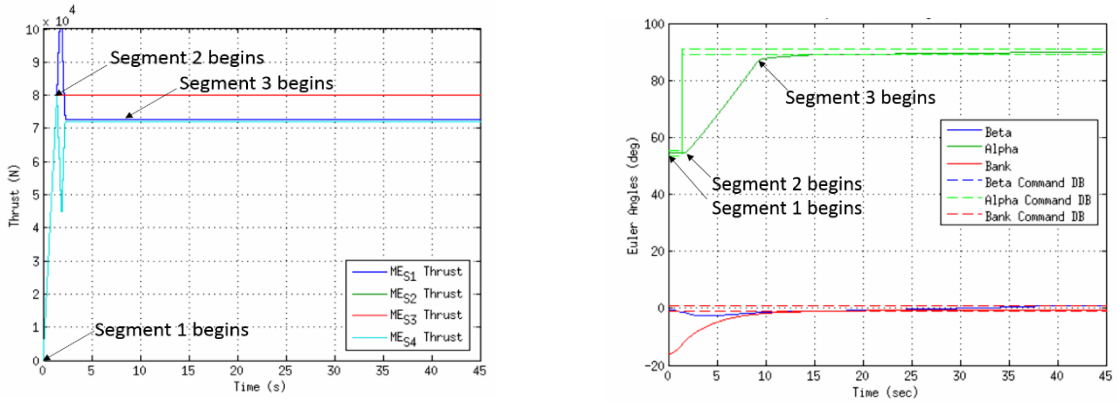

(a) Starboard Engine Thrust

(b) Attitude Performance

Figure 8. Descent Control System Performance (With Throttle Rate Limits)

DESCENT AND LANDING CONTROLLABILITY ROBUSTNESS

To assess the robustness of the guidance and control strategy, dispersions of the initial conditions and vehicle properties were applied for the descent and landing phases of the fully end-to-end 6DOF EDL nominal trajectory. Main engine and RCS control logic responsible for powered descent will be tested by including CG offset uncertainties, limited throttle rates, aerodynamic uncertainties, and main engine startup transients. Performance of the off-nominal case will be measured by increases in propellant usage, degradation of attitude precision, and deviations from the desired soft landing of zero velocity. Robustness of the entry control system is the focus of a future paper.

CG Offsets and Main Engine Startup Transient Dispersions

An assessment of performance in the presence of CG offsets was evaluated. While the MRV has flaps and RCS jets to provide trim adjustments in the presence of offsets during entry, the descent and landing phases of flight are unable to utilize the flaps due to the presumably main engine plume impingement on the flaps. As aforementioned, the RCS are inhibited in Segment 1 to allow the main engines to provide control in the presence of an offset. Main engine attitude control is later inhibited once the commanded thrust reaches a user defined lower thrust tolerance. One of the most detrimental uncertainties for control system performance is an unknown offset in CG locations. And despite the CG offsets, the RCS jets are still capable of providing attitude maintenance support for most of the descent and landing phase. The nominal CG location is for and X_{CG} of 10.5465 m from the nose and Z_{CG} of 1 m above the waterline shown in Figure 6. Main engine response to Y_{CG} and X_{CG} offsets at the maximum corners of the expected CG box is shown in Figure 9. Note that only an X_{CG} offset of 20 cm and a Y_{CG} offset of 5 cm are shown, since the MRV is most sensitive to offsets in these axes due to its geometry and mass distribution.

When using throttleable main engines, the speed at which the engine responds to commands is an important factor to consider for a higher fidelity 6DOF simulation. The timing of the powered descent through landing sequence is critical in achieving a soft touchdown. Because of this fact, the startup transient of the main engines was modeled to ensure that the control system could maintain the commanded attitude during this phase of variable thrust. Included in Segment 1 are main engine start up dispersions, where each main engine initial thrust value is randomly varied about a normal distribution of $\pm$ 3000 N. The RCS is inhibited in the beginning to allow main engines take out as much of the dispersions as possible until reaching the lower thrust command tolerance, when the main engines are inhibited allowing the RCS to take over.

In addition to the added challenge of startup transients, the control system also needed to be capable of handling the small differences in ramp up times and nominal thrust levels that may come from each engine. Figure 9a shows the effects of variable transient startup times and CG offsets, while Figure 9b shows little degradation in attitude tracking performance

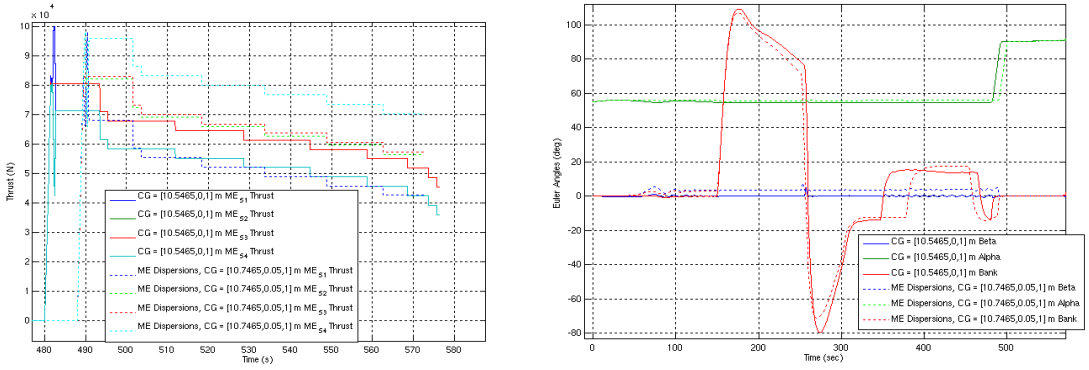

(a) Starboard Engine Thrust Comparison ***(b) Attitude Performance Comparison***

Figure 9. Control System Performance (Main Engine Transient Dispersions and CG Offsets)

End-to-end EDL Trajectory with Startup Transient Dispersions and CG Offsets

To fully stress the controls system performance and robustness, a fully end-to-end 6DOF trajectory was generated with descent and landing with all aforementioned dispersions were included. The results of the dispersed case (dotted lines) compared to the nominal case (solid lines) are shown in Figure 10. Figure 10a shows a deviation of only 1.8 m/s for the dispersed trajectory compared to the nominal soft landing solution trajectory. Constant thrust cases had deviations of larger than 30 m/s at the ground for its dispersed trajectory. Figure 10b shows the same small degradation in attitude tracking as Figure 9b. Figures 10c-10f show the increases in propellant usage and corresponding RCS jet output torques after these dispersions were applied. They show the propellant increases were primarily due to the CG uncertainty effects on the entry phase of flight.

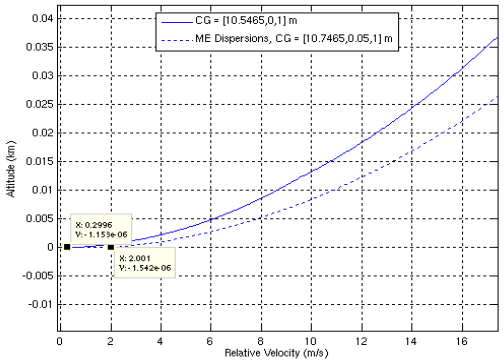

(a) Altitude vs. Velocity Comparison

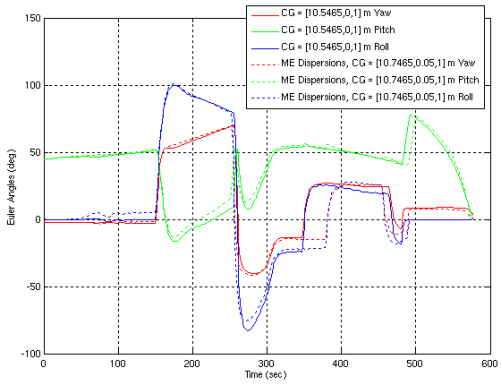

(b) Attitude Performance Comparison

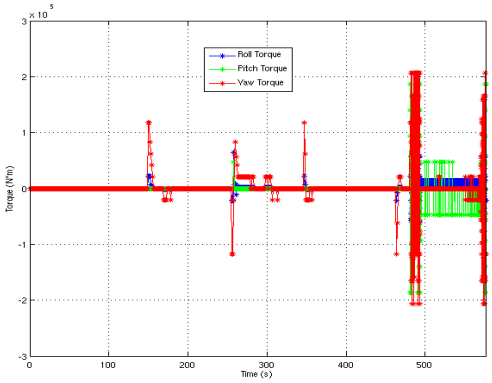

(c) RCS Jet Torques vs. Time (Nominal)

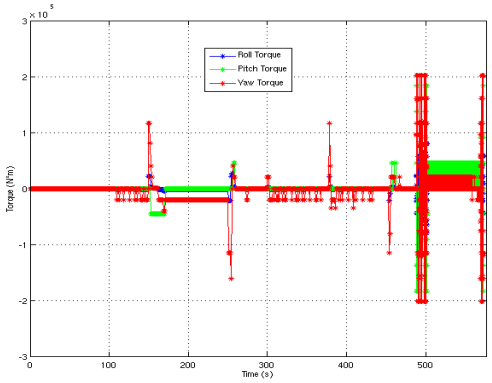

(d) RCS Jet Torques vs. Time (Off-Nominal)

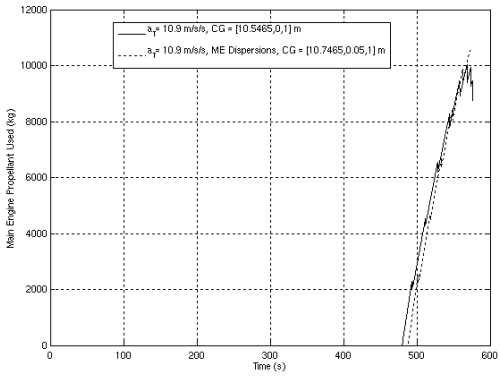

(e) Main Engine Propellant Used Comparison

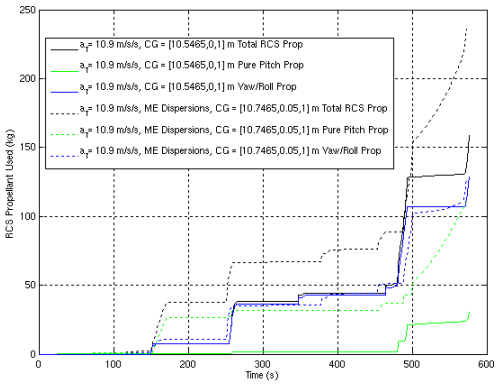

(f) RCS Propellant Used Comparison

Figure 10. End to End 6DOF Trajectory with CG Offsets and Main Engine Startup Dispersions.

CONCLUSION

A fully controllable 3DOF and 6DOF end-to-end trajectory has been presented for a nominal Mars trajectory. The successful simulated trajectory results imply that a combination of aerosurfaces, main engines, and RCS jets provide an effective control system design for the MRV. Lessons learned and assumptions made will provide insight into the considerations and decisions for not only the MRV but other candidate vehicles in the EMC study. While the control system response was successful in correcting dispersions and maintaining attitude, a more rigorous analysis of control system response with Monte Carlo simulation dispersions of aerodynamic coefficients, entry interface initial conditions, and engine dispersions for the entirety of EDL will be imperative in determining how well a constant acceleration Descent and Landing trajectory fares in targeting accuracy and achieving a soft landing. Future work also includes engine shutdown transient effects on performance during the vertical landing and improving propellant usage with gain tuning. The work presented demonstrates that the guidance and control strategy provides a feasible trajectory in landing a 20 mt payload to the surface of Mars, when no errors in navigated state are provided.

ACKNOWLEDGMENTS

The authors would like to acknowledge all the parties that contributed to the MRV 6-DOF simulation efforts including Phil Robinson, Edward Robertson, Daniel Matz, Joseph Garcia, Chuck Campbell, Alicia Cianciolo, Tara Polsgrove, and Francis Monahan.

NOTATION

a_T	=	constant thrust acceleration for the gravity turn
C_l, C_m, C_n	=	aerodynamic rolling, pitching, and yawing moment coefficients
g	=	acceleration due to gravity
h_0	=	height at the start of the gravity turn
I	=	moment of inertia
K	=	control system gain
L	=	aerodynamic reference length
M	=	Mach
p, q, r	=	inertial roll, pitch, and yaw rates
t	=	time
$\bar{q}$	=	dynamic pressure
S	=	aerodynamic reference area
V_0	=	velocity at the start of the gravity turn
α	=	angle of attack
β	=	sideslip angle
δ_a	=	aileron deflection
δ_e	=	elevon deflection
γ	=	flight path angle
μ	=	NED to body frame roll angle
ω	=	frequency
ϕ	=	bank angle
τ	=	torque
θ	=	NED to body frame pitch angle
ξ	=	damping ratio

REFERENCES

[1] Price, H., Manning, R., Sklyanskiy, E., Braun, R., "A High-Heritage Blunt-Body Entry, Descent, and Landing Concept for Human Mars Exploration", AIAA SciTech 2016, San Diego, CA, Jan 2016.

[2] Meginnis, I. M., Putnam, Z. R., Clark, I. G., Braun, R. D., Barton, G. H., "Guided Entry Performance of Low Ballistic Coefficient Vehicles at Mars", _Journal of Spacecraft and Rockets_, Vol. 50, No. 5, Sept.–Oct. 2013, pp. 1047-1059.

[3] Drake, B. G., "Human Exploration of Mars: Design Reference Architecture 5.0", NASA SP-2009-566, July 2009.

Entry, Descent, and Landing Systems Analysis Study: Phase 1 Report, NASA/TM-2010-216720 (2010).

Cianciolo, A. D., Polsgrove, T. T. "Human Mars Entry, Descent, and Landing Architecture Study Overview", SPACE 2016, AIAA 2016-5494.

[4] C. J. Cerimele, E. A. Robertson, R.R. Sostaric (editor), J. A. Garcia, "A Rigid, Mid-Lift-to-Drag Ratio Approach to Human Mars Entry, Descent, and Landing", AIAA SciTech 2017, Grapevine, TX, Jan. 2017.

[5] Lu, P., "Adaptive Powered Descent Initiation and Fuel-Optimal Guidance for Mars Applications", AIAA, SciTech 2018, Kissimmee, Florida.

[6] Lu, P., "Entry Guidance: A Unified Method", Journal of Guidance, Control, and Dynamics, Vol. 37, No. 3 (2014), pp. 713-728.

[7] "A Terminal Guidance Technique for Lunar Landing", S. Citron et. al, AIAA Journal, Vol. 2, No 3. 1964.

[8] Johnson, B., Cerimele, C., Stachowiak, S., Sostaric, R., Matz, D., Lu, P., "Mid-Lift-to-Drag Ratio Rigid Vehicle Control System and Simulation for Human Mars Entry", AIAA, SciTech 2018, Kissimmee, Florida.